Proceedings of ICFDP9:
Ninth International Congress of Fluid Dynamics & Propulsion
December 18-21, 2008, Alexandria, Egypt

ICFDP9-EG-269

NUMERICAL STUDY OF BUOYANCY – OPPOSED WALL JET FLOW

A. Abdel- Fattah
Associate Professor, Department of Mechanical Power Engineering, Faculty of Engineering
Menoufiya University, Shebin El-Kom, Egypt.

ashourabdelfatah@yahoo.com

ABSTRACT

This paper describes a numerical study of the flow and thermal fields for opposed wall jet. The hot water injected from plane jet down one wall of a vertical passage of rectangular cross section into cooled water which moves leisurely to the upper. The flow is assumed to be two dimensional, steady, incompressible and turbulent. The finite volume scheme is used to solve the continuity equation, momentum equations, energy equation and κ-ε model equations. The flow characteristics were studied by varying of Richardson number ($0.0 \leq Ri \geq 0.052$) and the ratio of back ground velocity to jet velocity ($0.05 \leq R \leq 0.15$). The results showed that, the buoyancy limited the downward penetration of the jet and its lateral spread when Richardson number increased. The shear layer formed at the interface between the two flow streams, and it becomes more concentrated at higher values of Richardson number. In this region, the intensity of the turbulence became stronger and the turbulent shear stress was a minimum value. When the velocity ratio increased, the penetration of jet decreases, its lateral spreading becomes less. Also the temperature difference decreases with the velocity ratio increases. The numerical results give good agreement with the experiment data of Ref. [1].

KEYWORDS: gas- cooled nuclear reactors, opposed flow jet, two dimensional turbulent jet, Re- circulation zone, turbulence production, heat transfer

1. INTRODUCTION

The study of the flow characteristics of a buoyancy opposed plane jet down a vertical wall is very important in certain gas- cooled nuclear reactors. The warm fluid leaves the core and it diverts down inside surface of a pressure vessel into a space containing with moving gradually or even stagnant cooler fluid. A number of works have been done on wall jets. However, the particular aspect of the topic studied in the present investigation, buoyancy-opposed wall jet flow, has received surprisingly little attention. The experimental study of buoyancy opposed wall jet flow was studied by He et al [1]. They measured the local velocity, turbulence intensities and temperature using Laser Doppler anemometry (LDA) and Thermocouples, in the flow field produced by a buoyancy-opposed wall jet discharging into a slowly moving counter-current stream in a vertical section of plane geometry. Their results showed, as Richardson number increased, the influence of buoyancy opposing the flow, had the effect on the downward penetration of the jet and its lateral spread. The progress in developing an analytical representation of the variation of dynamic variables and temperature across the near wall sub layer of turbulent flow was described by Craft et al. [2]. The aim of their study was the transport of heat and momentum to be packaged in the form of a wall function. Knowles and Myszko in their study [3] measured the mean velocity, turbulence intensities for a single circular, jet impinging onto a flat ground board. Fu and Tong [4] studied the influence of heat transfer rate of the heated wall in the channel with an oscillating cylinder. Their results indicated the effects of Reynolds number, oscillating amplitude, oscillating frequency, eccentric ratio, and blockage on the heat transfer characteristics

of the heat wall. The turbulence structure of an axisymmetric jet submerged in the co-flowing stream of the test section of a wind tunnel studied experimentally by Borean et al. [5]. They used petit tube and stationary hot wire for measuring the mean jet velocity and turbulence intensities for the jet flow. The unsteady turbulent flow of air and heat transfer in channel with a mounted square bar of different sizes detached from the wall were numerically by Valencia [6]. His results showed that the effect of Reynolds number and bar height to channel height on the local and global Nusselt numbers on the channel walls are strongly modified by the unsteady vortex shedding induced by the bar. Buresti el al. [7] used Laser Doppler anemometry (LDA) and hot- wire to obtain the axial, radial velocity components and the fluctuation of these velocities. Parneix et al [8] studied numerically, the cooling of heated pedestal mounted on a flat plate. They showed the effect of Reynolds number and the nozzle to pedestal distance on the heat transfer coefficient. Yang and Shyu [9] studied the fluid flow and heat transfer characteristics multiple impinging slot jets with an inclined confinement surface. Their numerical results showed that the maximum local Nusselt number and maximum pressure on the impinging surface move downstream while the inclination angle is increased. The experimental work a two-dimensional reattachment nozzle with a zero exit degree (SJR) studied by Narayanan et al. [10]. They showed that the pressure coefficient and Nusselt number as function of Reynolds number, the nozzle diameter, and the nozzle to surface spacing. Magi et al [11] were computed the spreading rate coefficient of round and plane jet by employing the Reynolds – averaged Navier- Stokes (RANS) equations and with the equation reduced to their boundary layers (BL) form. Loi and Lu [12] studied experimentally the effect of wall inclination on the mean flow in two dimensional wall jet. The influence of disk rotation, the distance from nozzle to disk and Reynolds number on the flow characteristics of an impinging jet were studied numerically by Abdel-Fattah [13]. His results showed that, when the centrifugal force increases, the radial normal stresses and the shear stresses are increasing.

The present paper introduces a steady two – dimensional turbulent flow of buoyancy opposed wall jet numerically. The effect of Richardson number and the ratio of background velocity to jet velocity on the mean velocity, temperature, turbulence fluctuations, penetration and lateral spread were studied.

2. MATHEMATICAL MODELS

The physical model used in this study is shown in Figure 1. The test section is a vertical passage of rectangular cross section (height *H* and width *L*). Plane jet of warm water issuing downwards from a gap with a wide b encountered a slowly ascending stream of cooler water.

The inlet velocity of warm jet V_J and temperature T_J are uniform. *To* facilitate the analysis, the following assumption is made.

The fluid is water and the flow field is two dimensional, incompressible and turbulent

Based on the characteristics scales of b_J, V_J, and T_c and T_J, the dimensionless variables are defined as follows.

$$x=\frac{\bar{x}}{b}\ ,\quad y=\frac{\bar{y}}{b},\quad u=\frac{\bar{u}}{V_J},\ v=\frac{\bar{v}}{V_J},\qquad p=\frac{\bar{p}}{\rho V_J^2},$$

$$k=\frac{\bar{k}}{V_J^2},\ \varepsilon=\frac{\bar{\varepsilon} b}{V_J^3}\ and\ T=\frac{\left(\bar{T}-\bar{T}_c\right)}{\left(T_J-\bar{T}_c\right)}$$

Where the over bar represents the dimensional quantities. According to the above assumptions and dimensionless variables, the dimensionless governing equations are expressed as the following equations.

Continuity equation

$$\frac{\partial u}{\partial x}+\frac{\partial v}{\partial y}=0 \tag{1}$$

Momentum equations:

$$u\frac{\partial u}{\partial x}+v\frac{\partial u}{\partial y}=-\frac{\partial p}{\partial x}+\frac{\partial}{\partial x}\left[\left(\frac{1}{\mathrm{Re}}+\frac{1}{\mathrm{Re}_t}\right)\frac{\partial u}{\partial x}\right]+$$
$$\frac{\partial}{\partial y}\left[\left(\frac{1}{\mathrm{Re}}+\frac{1}{\mathrm{Re}_t}\right)\frac{\partial u}{\partial y}\right]+\frac{\partial}{\partial x}\left(\frac{1}{\mathrm{Re}_t}\frac{\partial u}{\partial x}\right)+$$
$$\frac{\partial}{\partial y}\left(\frac{1}{\mathrm{Re}_t}\frac{\partial v}{\partial x}\right) \tag{2}$$

$$u\frac{\partial v}{\partial x}+v\frac{\partial v}{\partial y}=-\frac{\partial p}{\partial y}+\frac{\partial}{\partial x}\left[\left(\frac{1}{\mathrm{Re}}+\frac{1}{\mathrm{Re}_t}\right)\frac{\partial v}{\partial x}\right]$$
$$+\frac{\partial}{\partial y}\left[\left(\frac{1}{\mathrm{Re}}+\frac{1}{\mathrm{Re}_t}\right)\frac{\partial v}{\partial y}\right]+\frac{\partial}{\partial x}\left(\frac{1}{\mathrm{Re}_t}\frac{\partial u}{\partial y}\right)$$
$$+\frac{\partial}{\partial y}\left(\frac{1}{\mathrm{Re}_t}\frac{\partial v}{\partial y}\right)-\frac{Gr}{\mathrm{Re}^2} \qquad (3)$$

Energy equation

$$u\frac{\partial T}{\partial x}+v\frac{\partial T}{\partial y}=\frac{\partial}{\partial x}\left[\left(\frac{1}{\mathrm{Re\ Pr}}+\frac{1}{\mathrm{Re}_t\ \mathrm{Pr}_t}\right)\frac{\partial T}{\partial x}\right]+$$
$$\frac{\partial}{\partial y}\left[\left(\frac{1}{\mathrm{Re\ Pr}}+\frac{1}{\mathrm{Re\ Pr}_t}\right)\frac{\partial T}{\partial y}\right] \qquad (4)$$

The turbulent stresses are modeled as:

$$-\overline{u'v'}=\frac{1}{\mathrm{Re}_t}\left(\frac{\partial u}{\partial y}+\frac{\partial v}{\partial x}\right) \qquad (5)$$

$$-\overline{u}'^2=\frac{2}{\mathrm{Re}_t}\left(\frac{\partial u}{\partial x}\right)-\frac{2}{3}k \qquad (6)$$

$$-\overline{v}'^2=\frac{2}{\mathrm{Re}_t}\left(\frac{\partial v}{\partial y}\right)-\frac{2}{3}k \qquad (7)$$

where

$$\mu_t=c_\mu\frac{\rho\ k^2}{\varepsilon}$$

Here μ_t is the eddy viscosity, c_μ is a model constant, k is the turbulent kinetic energy, and ε is the dissipation rate of the turbulent kinetic energy. The transport equations for turbulent kinetic energy and its dissipation are given by:

$$u\frac{\partial k}{\partial x}+v\frac{\partial k}{\partial y}=\frac{\partial}{\partial x}\left[\left(\frac{1}{\mathrm{Re}}+\frac{1}{\sigma_k\ \mathrm{Re}_t}\right)\frac{\partial k}{\partial x}\right]$$
$$+\frac{\partial}{\partial y}\left[\left(\frac{1}{\mathrm{Re}}+\frac{1}{\sigma_k\ \mathrm{Re}_t}\right)\frac{\partial k}{\partial y}\right]+G-\varepsilon \qquad (8)$$

$$u\frac{\partial \varepsilon}{\partial x}+v\frac{\partial \varepsilon}{\partial y}=\frac{\partial}{\partial x}\left[\left(\frac{1}{\mathrm{Re}}+\frac{1}{\sigma_\varepsilon\ \mathrm{Re}_t}\right)\frac{\partial \varepsilon}{\partial x}\right]+$$
$$\frac{\partial}{\partial y}\left[\left(\frac{1}{\mathrm{Re}}+\frac{1}{\sigma_\varepsilon\ \mathrm{Re}_t}\right)\frac{\partial \varepsilon}{\partial y}\right]+c_1\frac{\varepsilon}{k}G-c_2\frac{\varepsilon^2}{k} \qquad (9)$$

Where G is the rate of production of k and is given by

$$G=\frac{1}{\mathrm{Re}_t}\left[\left(\frac{\partial u}{\partial y}+\frac{\partial v}{\partial x}\right)^2+2\left(\frac{\partial u}{\partial x}\right)^2+2\left(\frac{\partial v}{\partial y}\right)^2\right] \qquad (10)$$

The values of the model constants are taken as:
c_1=1.44 , c_2 = 1.92, c_3 = 1.373, c_μ =0.09, σ_k= 1 and σ_ε=1.3
The computational domain boundaries are shown in Fig. 2.
The boundary conditions for the above set of governing equations are as follows:
a) Inlet boundary (*a-b, g-h*)
The uniform velocity, temperature profiles and turbulent kinetic energy dissipation rate are
at *(a-b), i.e.*, $v=V_c$, $T=T_c$, k_c = *0.04* V_c^2 and ε_c = $\dfrac{c_\mu k_c^{1.5}}{0.1b_c}$

at *(g- h), i.e.,* $v=V_J$, $T=T_J$, k_J = *0.04* V_J^2 and ε_J = $\dfrac{c_\mu k_J^{1.5}}{0.1b_J}$

b) at walls *b-c , d-e, e-f , g-f and h-a*

The condition at solid wall are imposed *u = v = 0*. In the standard *k- ε* model, the velocity and temperature at the grids adjacent to wall are specified by wall function. The wall function are suggested by Launder and Spalding [14]

d) Exit boundary

A zero gradient condition is employed across the outlet boundary. Although this boundary condition is strictly valid only when flow is fully developed, it is also permissible for sufficient downstream from the region of interest, i.e., $\frac{\partial \phi}{\partial y} = 0$ and $\phi = u, v, T, k$ and ε

3. SOLUTION PROCEDURE

The governing differential equations for mass, momentum, energy, turbulent kinetic energy and its dissipation rate were solved using the control-volume-based finite difference method described by Patankar [15]. The SIMPLE algorithm [15] was used to resolve the pressure- velocity coupling. A 150 x 120 grid was placed non-uniformly in the computational domain. The x direction (stream wise) grids were chosen non-uniform, front the jet wall and were expanded out word by power low formulation with a power of 1.01. The y direction grid was chosen non-uniform, such that the finest grid was in side of wall jet and was expanded out word by power low formulation with a power of 1.03, see Fig. 2.

4. RESULTS AND DISCUSSION

Numerical investigations were carried out for Richardson number of ($0 \leq Ri \leq 0.052$), the Reynolds number of (Re = 4754) and the ratio of back ground velocity to jet velocity in range ($0.05 \leq R \leq 0.15$)

4.1. The Mean Flow Vector Fields

The mean velocity vectors fields at the ratio of back ground velocity to jet velocity (R = 0.0762) and different values of Richardson number (Ri = 0.0, and 0.02) is shown in figure 3. The isothermal condition (Ri = 0) is shown in figure 3(a) and the non-isothermal condition (Ri = 0.02) is shown in figure 3(b). This figure shows a range of buoyancy influence from frail to moderately strong. From this figure, it can be noticed that, for both cases, the jet flow spreads and decelerates then turns upwards and combines with counter –current stream and the united flow leaves the test section at the top. The jet flow penetrates left down to the bottom of test section. Also, it is seen that, the penetration of the jet and its lateral spread are reduced with increases of Richardson number, see Figure 3 (b).

When the ratio of back ground velocity to jet velocity was increased, the penetration of jet decreases. This is because the kinetic energy of counter – current increases, see Figure.3 (*c*) & (*d*).

4.2. The Vertical Component of Local Mean Velocity

Figure 4(*a*-*c*) declares the dimensionless of the vertical component of local mean velocity (v/ V_j) variation with changing the dimensionless distance (x/b) at different values of Richardson number, Each figure for different values of test section height. (H/b). From each figure, it can be seen that, the flow field consisted of three parts. First region is a wall jet region. In this region, the velocity is downwards and is comparatively large and decays as the test section height increases. This decay occurs more rapidly and the penetration of the jet is reduced by increasing Richardson number. The second region is the mixing region which occurs between the wall jet flow and the counter- current stream. In this region, the velocity reaches to zero after the edge of the jet front. The third zone is the return flow region, in this region; the flow turns upwards As Richardson number increases, the velocity profile also changes in this region. From figure 4(a), it can be seen that, the maximum upward velocity occurs near the far wall and decreases gradually with distance from that wall. The location of the maximum velocity in the return flow shifts away from the far wall by increasing Richardson number. In the middle of the test section, as results of the influence of buoyancy, which is significant in the region, the flow accelerates in this region

Figure.5 represents a graph of the downward velocity as function of test section height (H/b) at the distance from the jet wall of (L/*b* =0.78) for different values of Richardson number. From this figure, it is seen that, the velocity profile can be divided into the following regions the development region, the region of the counter- current flow and the mixing region. The development region is below the jet exit. In this region, the velocity decays comparatively slowly. Three stages can be identified. Below the jet exit there is a development region in which the velocity decays comparatively slowly. The down distance of the decays of the velocity depends on Richardson number. The decays of velocity become much greater due to mixing. When the velocity becomes negative, this indicates that the region of the counter- current flow has been reached. The greater the buoyancy effect occurs before the velocity variation changes from the first to the second stage. It can also be seen that, the steeper is the velocity variation within the mixing region at higher value of Richardson number. The velocity becomes zero quickly almost immediately below the jet injection location at highest value of Richardson number then the flow immediately turns and bends away from the wall.

The value of this velocity decreases with the increase of ratio of back ground velocity of counter-current stream inlet to the jet velocity (R). This is because the penetration of jet is reduced by increasing the kinetic energy of the counter-current stream inlet, see Figure 6.

4.3. The Turbulence Field

Figure 7 and Figure 8 represent a graph of the root – mean square values of the dimensionless for the turbulence velocity fluctuation, figure 7 for the vertical component of turbulent velocity fluctuation (v'/V_J) and figure 8 for the horizontal component of turbulent velocity fluctuation (u'/V_J). From These figures, it is noticed that, above the mixing region, the turbulence intensity is usually uniform. Same results are obtained in the re-circulation zone with low mean velocity. The normalized RMS velocities remain at a level similar to those in the other regions, mainly for strong buoyancy, the RMS velocities is improved in the jet frontal area. The higher levels of turbulence intensity occur in both the wall jet region and maxing region, even though the location of these regions of high turbulence shifts as a result of buoyancy effects. In the return flow region, also the buoyancy has effect. The turbulence intensity in this region is comparatively small for isothermal case, and also for case with weak buoyancy influence. At the location nearest the wall, the turbulent shear stress approaches zero and increases a little with distance from the wall. The minimum value of turbulent shear stress is occurred in the region near the far wall with strong buoyancy effect. This is depends on the mean velocity field. As Richardson number increase, the maximum upward velocity in the return flow region shifts away from the far wall then the gradient of mean velocity changes sign nearest that wall by increasing the buoyancy influence consequently, the shear stress also becomes minimum.

4.4. The Temperature Field

Figure 9 shows the local mean temperature down the jet wall as a function of the test section height for different values of Richardson number at constant value of the ratio of back ground velocity to jet (R= 0.0762) and constant value of Reynolds number (4754).From this figure, it is seen that, the trend of the wall temperature is similar to the trend of the mean velocity in jet flow, see figure 5. At the first, the temperature decays slowly and reaches to zero quickly within a short distance to that of the counter-current flow. The short distance for higher temperature decreases by increasing Richardson number. Also, it can be noticed that, the trend of the temperature above the region of higher temperature is similar for each cases of the trend of the mean velocity, see figure 5.
As the buoyancy influence increases, the hot jet fluid is limited to a little region; there is a small variation of temperature across the jet flow even for the case with the higher value of Richardson number, consequently, the buoyancy has a small effect on the flow within jet. Also the trend of the temperature is similar by increasing of the ratio of the background velocity to the jet velocity. See Fig 10. This is because the increase of (*R)*, the increment of restricting increases.

4.5. Jet Penetration

Figure 11 shows the jet penetration as a function of Richardson number at different values of the ratio of back ground velocity to jet velocity (R). The definition of the penetration of the jet is determined by the distance from the jet exit to the location at which the normalized value of wall jet temperature equals background stream temperature. From this figure, it is seen that the jet penetration reduces with the increase of the Richardson number. This is because the buoyancy force increases with Richardson number increase. Also the jet penetration decreases with the ratio of back ground velocity to jet velocity (R) increases. That is the increment of the ratio of background velocity to jet velocity was a controller for the jet velocity.
Figure 12 shows the lateral spread of the jet as a function of Richardson number at different values of the ratio of back ground velocity to jet (R). The definition of the lateral spread of the jet is determined by the distance from the jet wall to the location where the maximum vertical component of velocity occurs. This distance generally is changeable with height.
From this figure, it is noticed that the scatter of the points is comparatively large. This is because, the velocity profiles were very flat in some cases consequently, it is difficult to decide exactly on the location at which the maximum velocity was achieved. Also, it can be noticed that, the lateral spread decreases with increase of Richardson number. The figure also show that the lateral spread reduces by increasing of the ratio of back ground velocity to jet (R).

5. CONCLUSIONS

The major conclusions of this research could be summarized as follows:

The flow field can be considered in three parts, a wall flow region, a mixing region between the wall jet flow and the counter- current stream and return flow region. In the wall jet region, the vertical component of local mean velocity is reduced height. With the increase of Richardson number, this decay becomes more quickly and it falls to zero in the mixing region. With increase of Richardson number, the velocity profile in the return flow region changes. The temperature decreases by increasing the Richardson number and /or the ratio of back ground velocity to velocity jet increase. The penetration of the jet and the lateral spread of the jet reduce by increasing of Richardson number also by increasing of the ratio of back ground velocity to jet velocity. The comparison between the numerical results and experimental measurements [1] gives good agreement.

NOMENCLATURE

b inlet width of exhaust nozzle

c_1, c_2 , c_3, c_μ, empirical constants
g gravitational acceleration
H test section height
Gr Grashof number ($Gr = \frac{gb^3(\rho_c - \rho_J)}{\rho v_j^2}$)
k turbulent kinetic energy
L test section width
p pressure
Pr Prandtl number
Pr_t turbulent Prandtl number
R velocity ratio(= V_c/V_J)
Re Reynolds number ($Re=\rho V_J b /\mu$)
Re_t turbulent Reynolds number ($Re_t = \rho V_J b/\mu_t$)
Ri Richardson number ($Ri = \frac{gb\ (\rho_c - \rho_J)}{\rho V_j^2}$)
T temperature
u` horizontal component of RMS turbulent fluctuation velocity
u horizontal component of local mean velocity
u' ύ turbulent shear stress
ύ vertical component of RMS turbulent fluctuation velocity
v vertical component of local mean velocity
V_J average velocity at the jet injection location
x, y Cartesian coordinates

Greeks letters

β ateral spread of jet
δ jet penetration distance
ε rate of dissipation of k
μ dynamic viscosity
ν kinematic viscosity
ρ density
σ_ε model constant
σ_κ model constant

Subscripts

c counter- current stream inlet
j jet exit
i indices for turbulent

REFERENCES

[1] S. He, Z. Xu, and J.D. Jackson, J, " An Experimental Investigation of Buoyancy- Opposed Wall Jet Flow", International Journal of Heat and Fluid Flow, vol. 23, pp. 487-496, 2002.

[2] T. j. Craft, A. V. Geransmov, H. Lacovides, and B.E. Launder, "Progress in the Generalization of Wall- Function Treatments", International Journal of Heat and Fluid Flow, vol. 23, pp. 148-160, 2002.

[3] K. Knowles, and M. Myszko, "Turbulence Measurements in Radial Wall Jets", Experimental Thermal and Fluid Science, vol. 17, pp. 71-78, 1998.

[4] W. S. Fu, and B.H. Tong, "Numerical Investigation of Heat Transfer of a Heated Channel with an Oscillating Cylinder", Numerical Heat Transfer Part A, vol. 43, pp. 639-658, 2003.

[5] J.L. Borean, D. Huilier, and H. Burnange, "On the Effect of a Co- flowing Stream on the Structure of an Axisymmetric Turbulent Jet", Experimental Thermal and Fluid Science, vol. 17, pp. 10-17, 1998

[6] A. Valencia, "Turbulent Flow and Heat Transfer in a Channel with a Square Bar Detached from the Wall", Numerical Heat Transfer Part A, vol. 37, pp. 289-306, 2000.

[7] Buresti, Petagna and A. Talamelli, "Experimental Investigation on the Turbulent Near- Field of Coaxial Jets", Experimental Thermal and Fluid Science, vol. 17, pp. 16-28.1998.

[8] S. Parneix, M. Behnia, and P.A. Durbin," Predictions of Turbulent Heat Transfer in an Axisymmetric jet Impinging on a Heated Pedestal", Journal Heat Transfer, vol. 121, pp. 43-49, 1999

[9] Y. Yang, and C. Shyu, "Numerical Study of Multiple Impinging slot Jets with an Inclined Confinement Surface", Numerical Heat Transfer Part A, vol. 33, pp. 23-37, 1998

[10] V. Narayanan, J.S. Yagoobi, and R.H. Page, "Heat Transfer Characteristics of Slot Jet Reattachment Nozzle", Journal of Fluids Engineering Transaction of the ASME, vol. 120, pp. 348-355, 1998.

[11] V. Magi, V. Iyer, and J. Abraham, "The k-ε Model and Computed Spreading Rates in Round and Plane Jets", Numerical Heat Transfer Part A, vol. 40, pp. 317-334, 2001.

[12] C.S. Loi, and D. Lu. "Effect of Wall Inclination on the Mean Flow and Turbulence Characteristics in a Two Dimensional Wall Jet", Int. J. Heat and Fluid Flow, vol. 17, pp. 377-385, 1996.

[13] A.Abdel. Fattah, "Numerical Simulation of Turbulent Impinging Jet on a Rotating Disk", Int. J. Numerical Methods in Fluids, vol. 53(11), pp.1673-1688, 2007.

[14] B. E. Launder, and D.B. Spalding, "The Numerical Computation of Turbulent Flow, Comput. Methods Appl. Mech. Eng., vol 3, 269-289, 1974.

[15] Patankar, S.V., "Numerical Heat Transfer and Fluid

Flow, McGraw-Hill, New York, 1980.

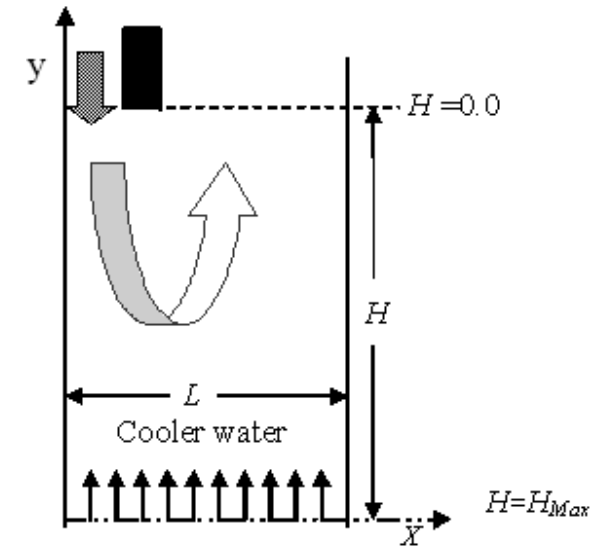

Fig. 1 Side view of test section

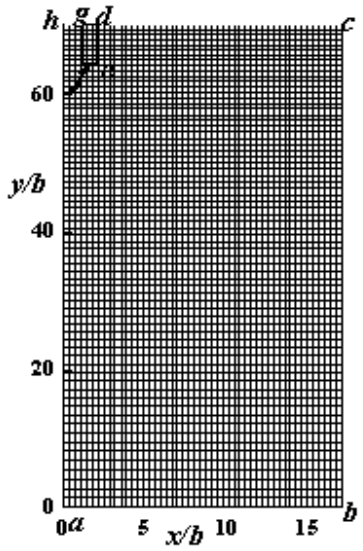

Fig. 2 Grid distribution

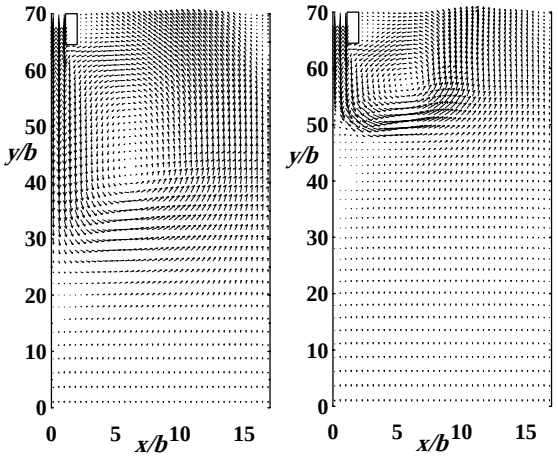

(*a*) *Ri* =0.0, *R* = 0.0762 **(*b*) *Ri* =0.02, *R* = 0.0762**

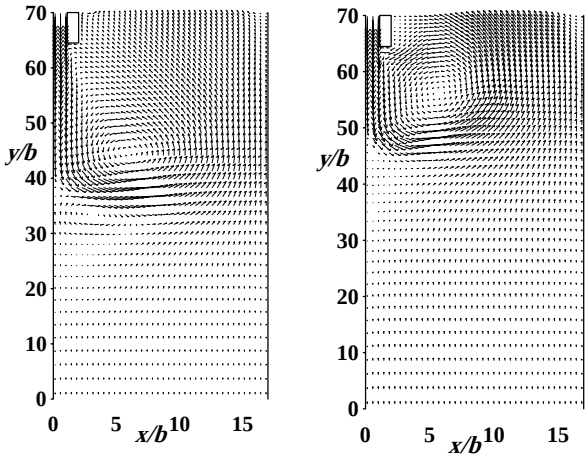

***(c)* *Ri* =0.01, *R* = 0.0762** **(*d*) *Ri* =0.01, *R* =0.12**

Fig.3 Mean velocity vector field at ***Re*** = 4754

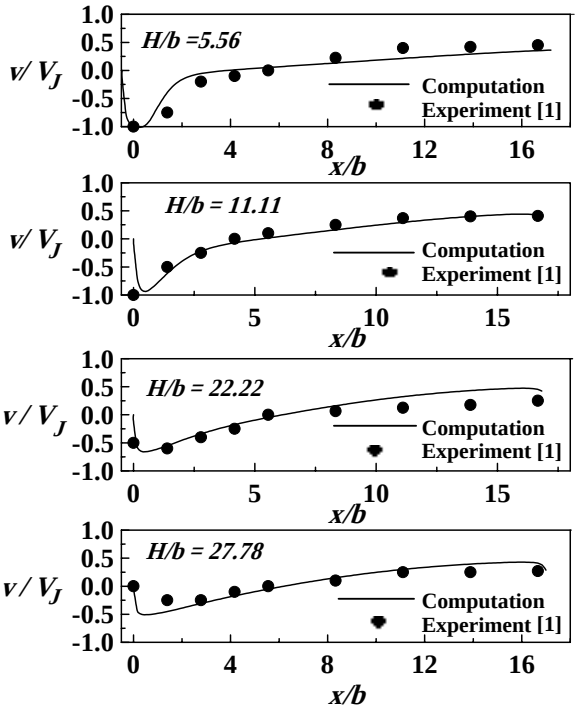

(*a*) *Ri* = 0.0

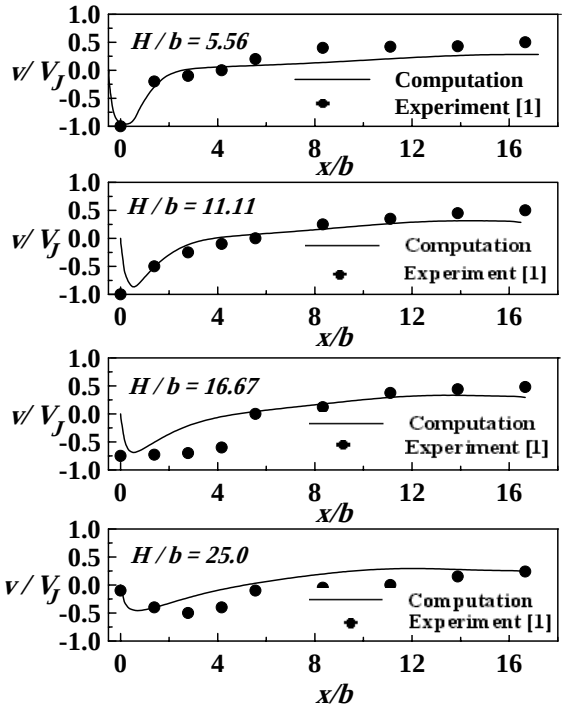

(*b*) *Ri* = 0.01

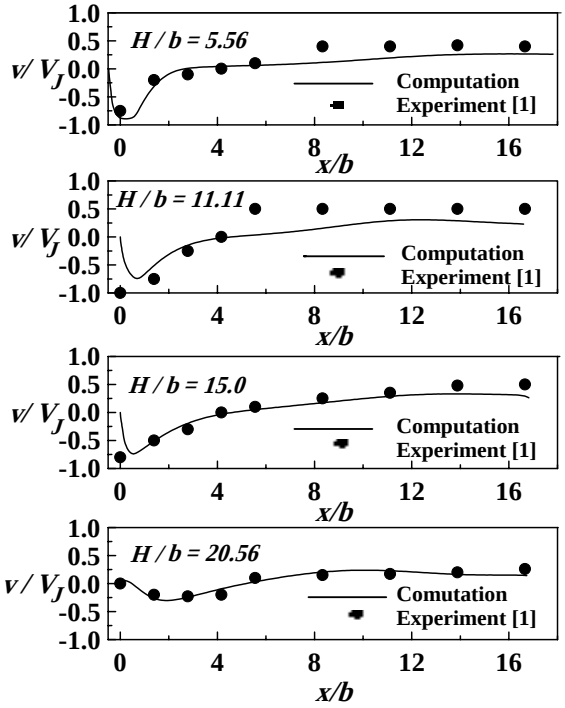

(*c*) *Ri* = 0.02

Fig. 4 Profiles of values of vertical component of local mean velocity at *Re* = 4754

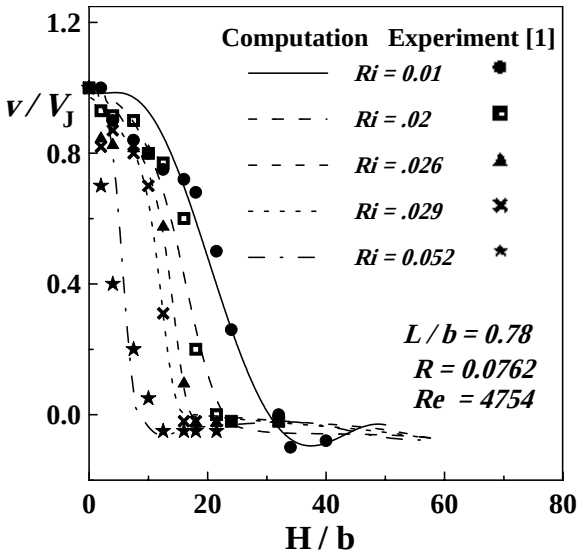

Fig .5 Variation of vertical velocity with Richardson number

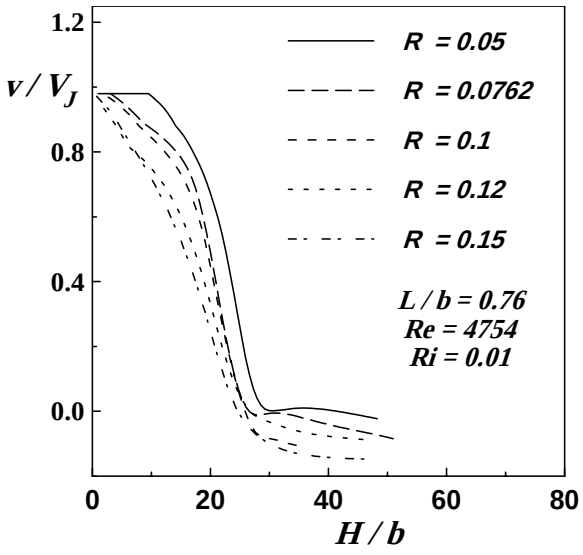

Fig. 6 Variation of vertical velocity with v_c/V_J

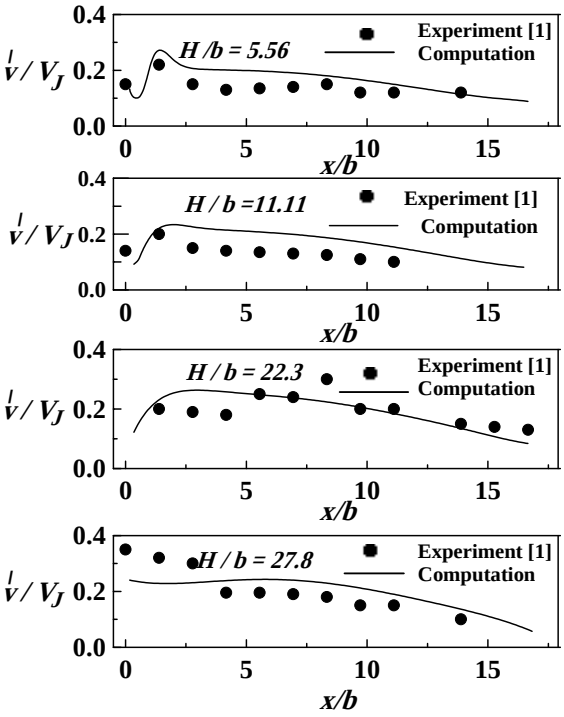

(*a*) *Ri* = 0.0

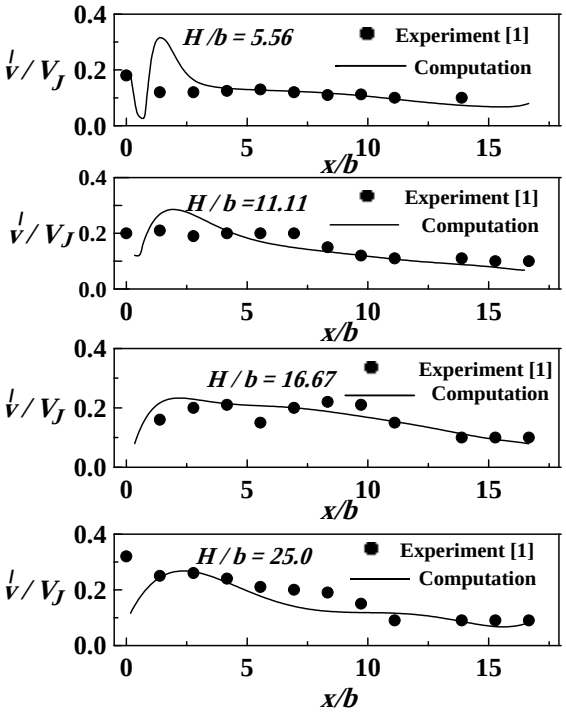

(*b*) *Ri* = 0.01

Fig.7 Profiles of vertical component of local RMS velocity fluctuation at *Re* = 4754 continued

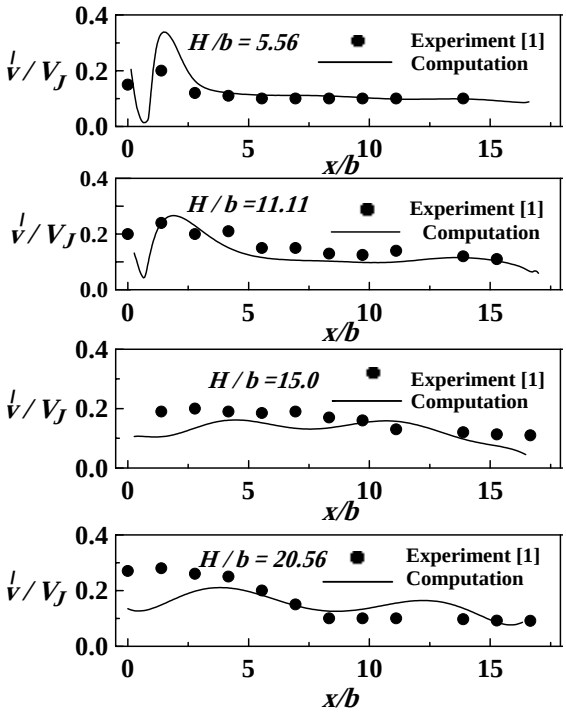

(*c*) *Ri* = 0.02

Fig.7 Profiles of vertical component of local RMS velocity fluctuation at *Re* = 4754

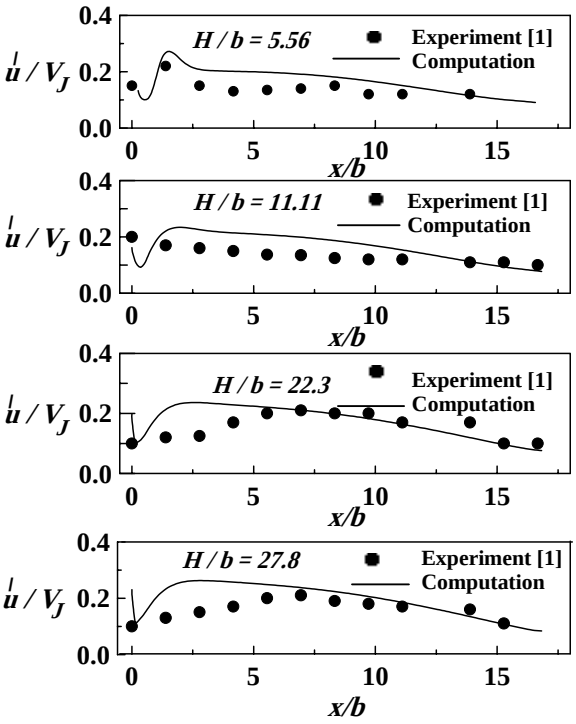

(*a*) *Ri* = 0.0

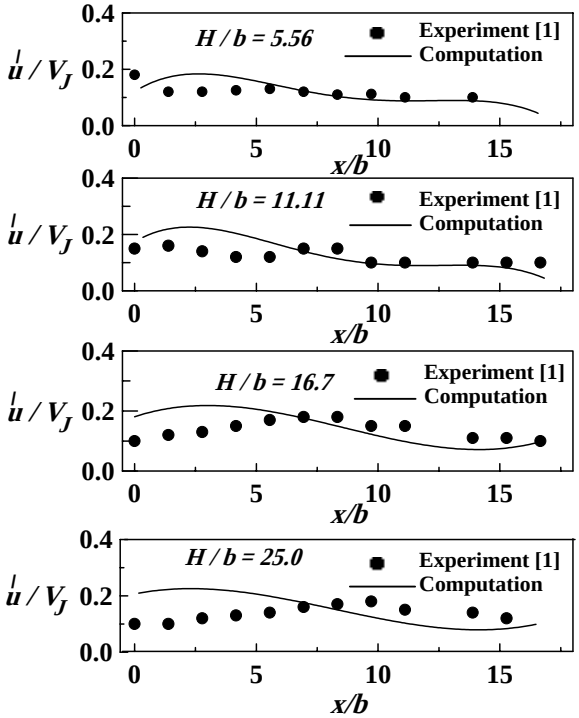

(*b*) *Ri* = 0.01

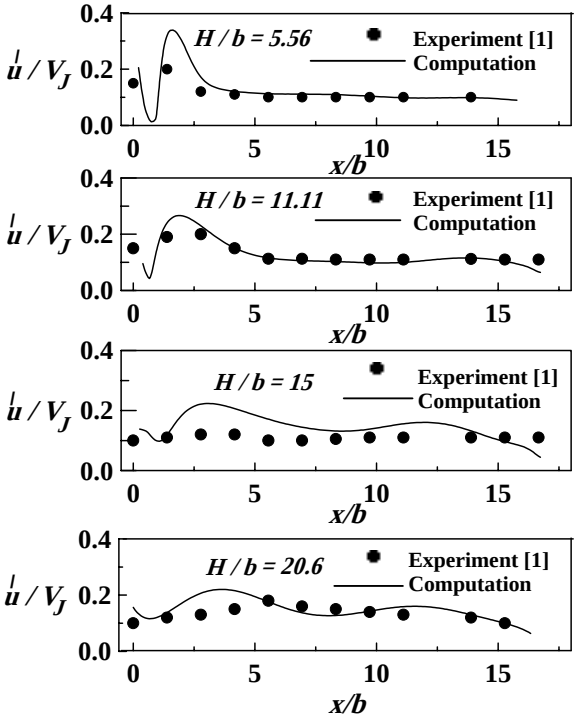

(*c*) *Ri* = 0.02

Fig.8 Profiles of horizontal component of local RMS velocity fluctuation at *Re* = 4754

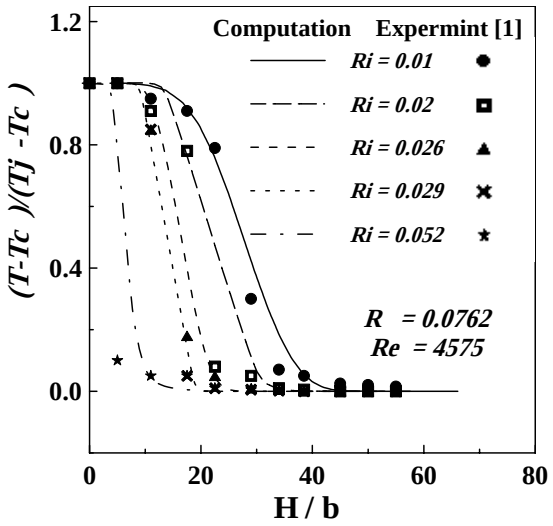

Fig. 9 Variation of wall temperature with Richardson number

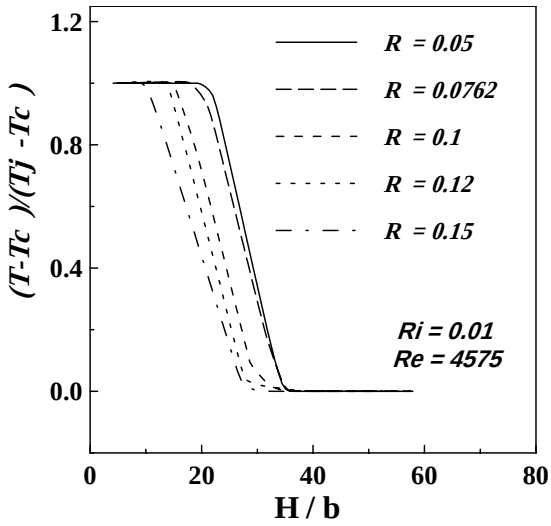

Fig. 10 Variation of wall temperature with v_c/V_J

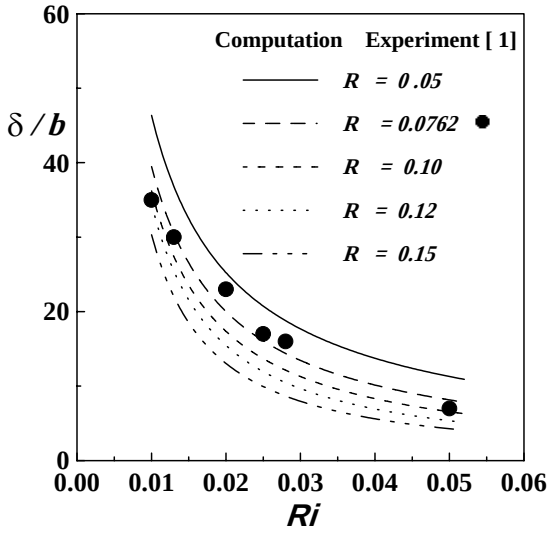

Fig. 11 Penetration of jet

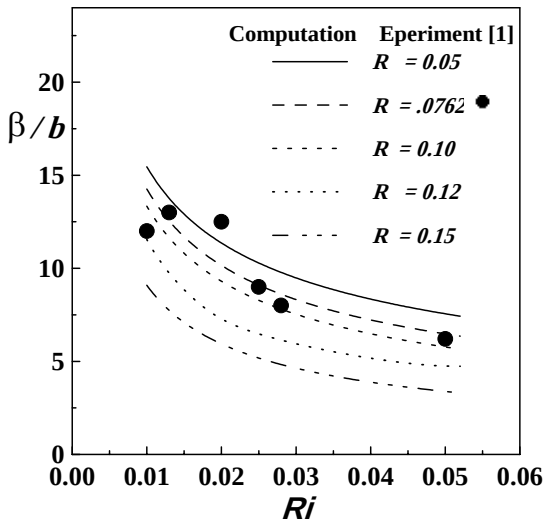

Fig.12 Lateral of jet